Wind and Structures, *Vol. 32, No. 1 (2021) 1-9*
DOI: https://doi.org/10.12989/was.2021.32.1.1

Effects of vortex generators on the wind load of a flat roof: A computational study

Yagebai Zhao[1,2a], Xiaolong Deng[1,2b], Hongfu Zhang[1,2c], Dabo Xin*[1,2] and Zhiwen Liu[3e]

[1]School of Civil Engineering, Northeast Forestry University, Harbin 150040, China
[2]Lab of Disaster prevention and reduction, Northeast Forestry University, Harbin 150040, China
[3]Hunan Provincial Key Laboratory of Wind Engineering and Bridge Engineering, Hunan University, Changsha Hunan, 410082, China

(*Received June 21, 2019, Revised February 10, 2020, Accepted December 21, 2020*)

Abstract. Vortex generators are commonly used in mechanical engineering and the aerospace industry to suppress flow separation owing to their advantages of simple structure, economic viability, and high level of efficiency. Owing to the flow separation of the incoming wind on the leading edge, a suction area is formed on the roof surface, which results in a lifting effect on the roof. In this research, vortex generators were installed on the windward surface of a flat roof and used to disturb to roof flow field and reduced suction based on flow control theory. Computational fluid dynamics (CFD) simulations were performed in this study to investigate the effects of vortex generators on reduce suction. It was determined that when the vortex generator was installed on the top of the roof on the windward surface, it had a significant control effect on reduce suction on the roof leading edge. In addition, the influence of parameters such as size, placement interval, and placement position of the vortex generator on the control effect of the roof's suction is also discussed.

Keywords: CFD (computational fluid dynamics); pressure distribution; roof structure; flow control; vortex generator

1. Introduction

With the development of building construction technology and new high-strength lightweight materials, roof spans are exhibiting an increasing trend. Also, with increasing building spans, the wind sensitivity of the roofs is enhanced. As a result, the wind load characteristics of roof structures are gradually becoming one of the key issues in the design of large span roofs. On 22 November 2011, the roof in the D area of the Beijing T3 terminal building was partially blown away causing property damage by strong winds with speeds of 24 m/s. In the early morning of 11 October 2018, Hurricane Michael landed in the United States with a pressure of 919 millibar at the centre of the hurricane. The US military stationed at the Yandel Air Base in Florida was significantly impacted by the hurricane and the roof of the base building was blown away by the wind.

Roof damage is caused by negative wind pressure in some areas of the roof that produces a strong suction force. Therefore, determining how to increase the negative wind pressure is an important aspect for ensuring the structural safety of a building's roof. The negative wind pressure stems from wind flow separation on the surface of the bluff body, which is often accompanied by the reattachment phenomenon (Cheng *et al*. 2000). Wind flow separation often occurs on bulging geometrical-shaped areas such as eaves, ridges, roof edges, and corners. The minimum negative wind pressure contributes a strong wind suction force on the roof surface, which can damage some of the roofboarding. Moreseriously, wind suction can cause roofboarding to be blown away. Based on the evidence presented above, it is critical to suppress wind flow separation in order to reduce the negative wind pressure, especially in the leading edge areas of the roof. Recently, researchers have numerically and experimentally analyzed the effect of changing shape and size parameters on the wind pressure coefficient using typical roofs as objects.

At present, wind resistance methods for roof structures are mainly based on changing the roof shape. Moravej *et al*. (2017) experimentally studied the influence of the height variations of a triangular roof and a four-slope roof on the wind pressure coefficient. The results showed that the peak wind pressure coefficient on the gable roof and the speed ratio between local velocities and oncoming flow velocities at the mean roof elevations did not change significantly with the building height, while the wind pressure coefficient at the corner of the temple roof greatly increased with height. Rizzo and Ricciardelli (2017) proved that the wind pressure coefficient of a hyperbolic parabolic roof was very sensitive to geometrical changes. Gullbrekken *et al*. (2018) established the relationship between the wind pressure coefficient with the structural form of the roof air-inlet and roof angle, by performing a full-scale wind tunnel test on a Norwegian building model. Shan, Tamura *et al*. (2018) carried out a wind tunnel test to study the effect of curved

*Corresponding author, Professor
E-mail: xindabo@nefu.edu.cn
[a]Ph.D. Student
E-mail: yagebai@nefu.edu.com
[b]M.Sc.
E-mail: hero19950611@hotmail.com
[c]Ph.D.
E-mail: hongfu2233@126.com

ISSN: 1226-6116 (Print), 1598-6225 (Online)

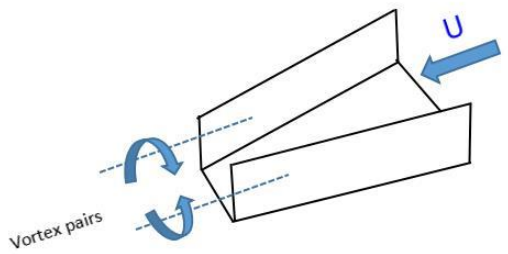

Fig. 1 Schematic diagram of the operation principle of a vortex generator

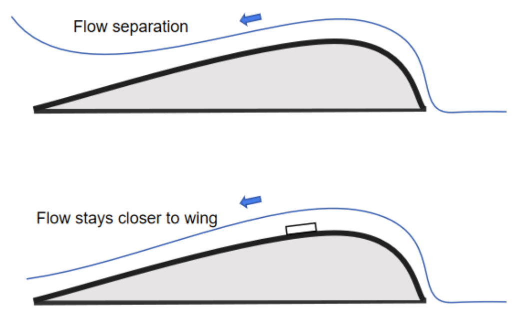

Fig. 2 Premature flow separation suppressed by vortex generators

slopes, high ridges, and double shackles on wind pressure by focusing on traditional Chinese temple roofs, including protruding ridged roofs and non-protruding ridged roofs. The experimental results indicated that the high ridge size of the former protruding ridge roof affected the distribution of the mean and peak wind pressure coefficients considerably. Recently, the development of flow control methods by purposely improving wind field characteristics are on the rise. One kind of flow control method involves optimising the placement of structural attachment equipment. Structural engineers often use a low-profile wall at the edge of a flat roof to lift the vortex from the corner area off the roof. For example, Browne, Gibbons *et al*. (2013) placed low retaining walls on tilted solar roofs to shift the vortex shedding away from the roof. Further, structural engineers optimized the chimney position to suppress flow separation and increase the negative wind pressure (Oliveira 2018). Another type of flow control method arranges a special device that can actively or passively generate a vortex to disturb the oncoming wind flow and thereby increase the minimum negative wind pressure.

A passive vortex generator (PVG) is a simple and effective piece of flow control equipment that can generate a pair of downstream vortexes in the boundary layer, as shown in Fig. 1. The PVG can promote the exchange of momentum in the upper and lower boundary layers, so as to enhance the fluid momentum at the bottom of the boundary layer and balance the boundary layer velocity profile. Consequently, the boundary layer separation is delayed (Manolesos and Voutsinas 2015) as shown in Fig. 2. As a

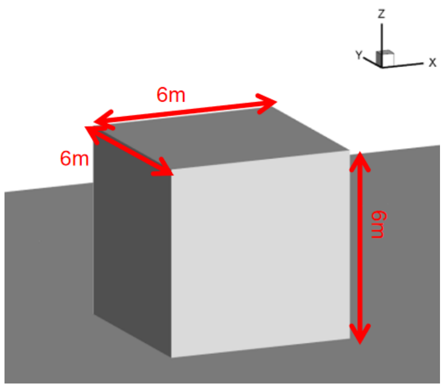

Fig. 3 Model size

boundary layer separation suppression equipment, the PVG has been widely used to control the boundary in internal and external flow fields (Lin 2002).

The research on PVG was first developed in the aviation and mechanical engineering fields. Lin (2002) found that passive vortex generators could produce downstream vortices that control boundary layer separation and improve the aerodynamic performance of airfoils. Stillfried, Wallin *et al*. (2010) proposed an improved vortex generator model that had a better effect on controlling the flow separation in the boundary layer. Gao *et al*. (2016) determined the flow control characteristics of several types of micro-vortex generators under the condition of Mach number 2.0 asymmetric flow by numerical simulation.

In the field of structural wind engineering, Xin, Zhang *et al*. (2018) carried out an experimental study on mitigating the vortex-induced vibrations of a bridge using PVGs. The results showed that the vortex generators can completely suppress the vortex shedding near the wake, which leads to the disappearance of wind-induced vibrations.

The purpose of this research was to use vortex generators (VGs) to suppress flow separation and increase the negative wind pressure of a flat roof. The vortex generators were installed on the windward surface to disturb the flow field, which can increase the negative wind pressure on the leading edge of the roof. As computational fluid dynamics (CFD) is an effective method for structural wind engineering simulations (Lee 2000), this research utilised CFD numerical simulations to verify the effect of the VGs at increasing the negative wind pressure on the roof.

2 Parameters of the flat roof model and vortex generators

2.1 Model parameters of the flat roof

The model and dimensions of a typical flat roof are shown in Fig. 3.

The cube bluff body is always taken as the simple test model with a side length of 6 m (Richards, Hoxey *et al*. 2001). The results of the wind tunnel experiments and numerical simulations of this cube can be found in many references (Baetke, Werner *et al*. 1990).

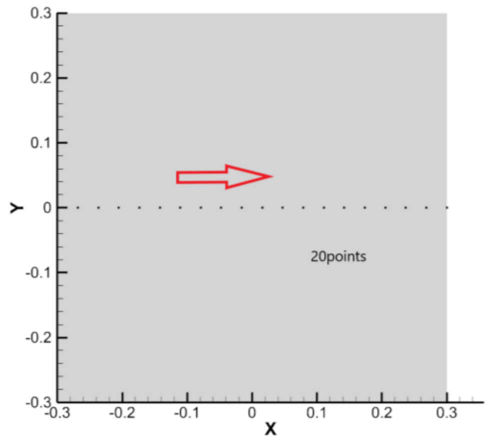

Fig. 4 Location of the measuring points and wind speed direction

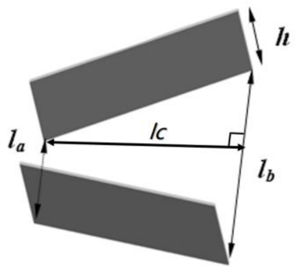

Fig. 5 Dimension diagram of a vortex generator

In this study, a cube model with a length of 6 m was adopted and the scale ratio was 1/10. The measuring points were arranged on a flat roof of 0.6 m × 0.6 m. There were 20 equidistant points for obtaining wind load data measurements on the centre line (y = 0) of the roof. The positions of these measuring points are shown in Fig. 4. The wind pressure (Pa) and the wind velocity magnitude (m/s) at the measuring points were investigated. Similarly, on the y = 0 centre line of the windward surface and the y = 0 centre line of the leeward side, there were 20 equidistant measuring points (Beyers, Sundsbø*et al*. 2004).

2.2 Parameters of the vortex generator model

The dimensions of the vortex generator used in numerical simulations are shown in Figs. 5 and 6, where l_a is the leading edge distance of the vortex generator, l_b is the trailing edge distance of the vortex generator, l_c is the vertical distance between the leading edge and the trailing edge of the vortex generator, h is the height of the vortex generator, λ is the horizontal distance between the vortex generators, and θ is the angle between the vortex generator and the incoming flow.

The parameter assignment of the VGs in the present study's simulation is shown in Table 1. The specific working conditions and simulation results will be discussed in Section 4. The influence of the row numbers of the VGs on the flow field of the flat roof were studied using this numerical simulation. The installation location of vortex

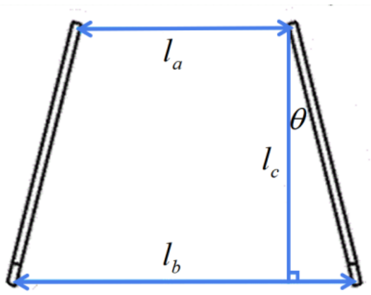

Fig. 6 Overview of vortex generator dimensions

Table. 1 Parameters of the VGs in the simulation

l_a	0.02 m
l_b	0.06 m
l_c	0.04 m, 0.06 m, 0.08 m
h	0.01 m, 0.02 m, 0.03 m, 0.04 m, 0.05 m
λ	0.1 m, 0.25 m
θ	18°

generators is shown in Fig. 7. d is equal to 0.1 m, which is the vertical distance between the top and bottom rows of the VGs.

3. Numerical simulation method

3.1 Computational mesh

As shown in Fig. 8, the computational domain had a length of 12.6 m, width of 3.6 m, height of 3.6 m, and blocking ratio of 2.78%. The mesh type used in the simulation was a hybrid mesh, which included a tetrahedral mesh and hexahedron mesh. As identified in the figure, the computational domain is divided into two regions. The inside zone was named Zone 1 and the outside zone was Zone 2. There were two kinds of numerical simulations, including a numerical simulation without a vortex generator installed and a numerical simulation with the VG model installed on the top of the windward surface.

For the numerical simulation of the flat roof where the VGs were not installed, Zone1, was set as the refinement area to ensure the accuracy of the simulation. The refinement area was determined using a structured mesh of size 0.3 m, and the Zone2 area was revealed using a structured mesh of size 0.8 m. For the numerical simulation of the flat roof with the vortex generator model installed, Zone1 was also set as the refinement area in order to ensure the accuracy of the calculation. For the mesh refinement area, a 0.01 m size tetrahedral mesh was generated near the vortex generator, a tetrahedral mesh with a mesh size of 0.1 m was generated on the surface of the building, and a mesh size of 0.8 m was generated in the remaining refinement regions. For the Zone2 area, a hexahedral structured mesh of size 0.8 m was generated, as shown in Fig. 9. In the computational domain, the interface pair was used for data transfer between the boundary areas of Zone1 and Zone2.

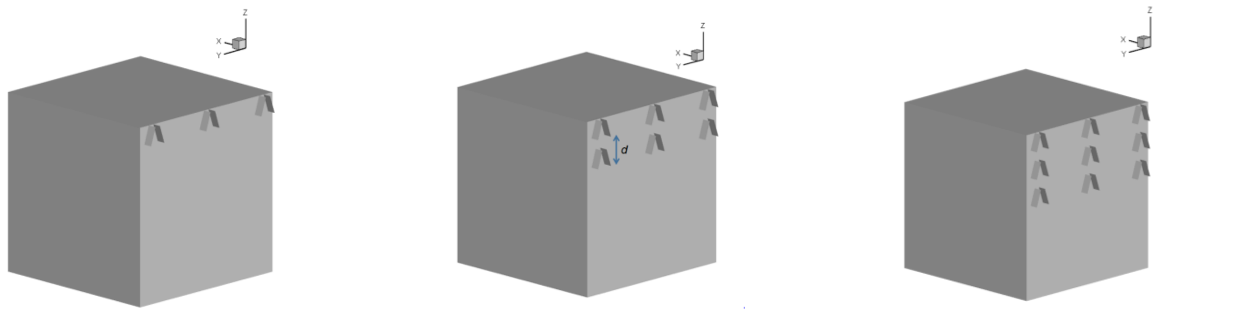

(a) Placement of a row of vortex generators (b) Placement of two rows of vortex generators (c) Placement of three rows of vortex generators

Fig. 7 Schematic diagram of adjusting the row numbers of the VGs

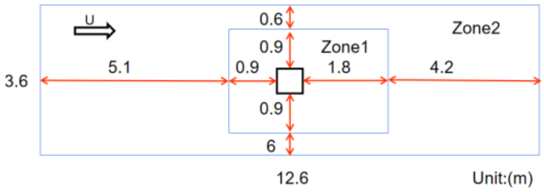

Fig. 8 Computational domain

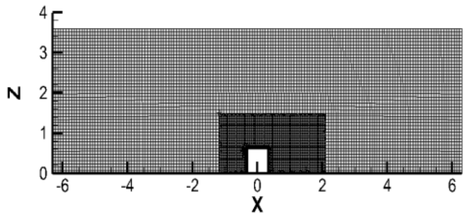

Fig. 9 Computational mesh

The global diagram of the computational domain is shown in Fig. 10 and the computational mesh of the VG and the windward surface are shown in Fig. 11. The local mesh of the VG is shown in Fig. 12.

3.2 Boundary conditions and numerical strategy

The turbulence model based on Shear Stress Transport (SST) was used to solve Navier–Stokes (N-S) equations in the numerical simulation of the flat roof. The equation is discrete in space by the finite volume method, and the time integral scheme was adopted in the second order implicit scheme. The coupled iterative method of the pressure and velocity fields was adopted using the SIMPLEC algorithm. The Fluent simulation software was utilised.

The inlet boundary adopts velocity inlet boundary conditions. The user defined formula (UDF) was used to simulate the atmospheric boundary layer wind profile at the entrance of the computational domain. The wind speed formula based on logarithm Eq. (1) was used to simulate the atmospheric boundary layer (Blocken, Statshopoulos *et al.* 2007). The wind profile is shown in Fig. 13.

$$U(z) = \frac{u^*}{\kappa} \ln\left(\frac{z+z_0}{z_0}\right) \tag{1}$$

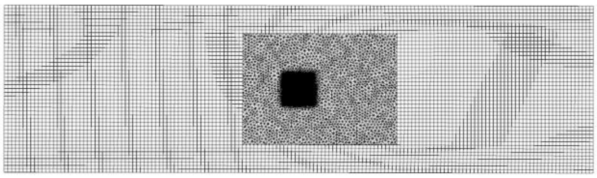

Fig. 10 Schematic diagram of the global grid division of the computational domain

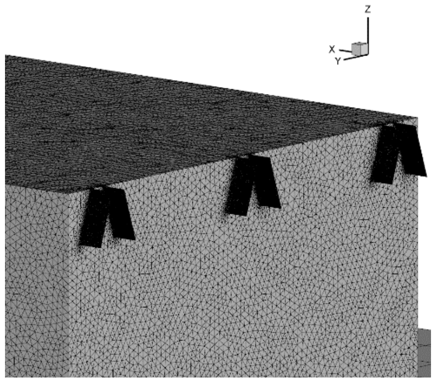

Fig. 11 Computational mesh of the VGs and the windward surface

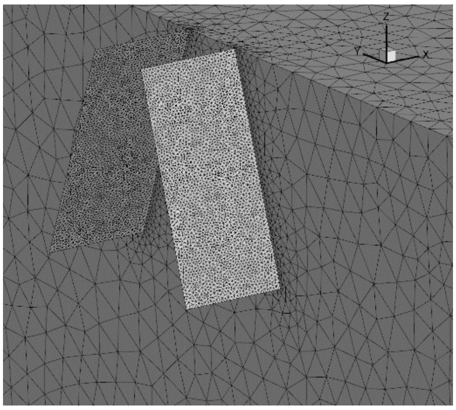

Fig. 12 Local grid generation of the VGs

where, κ is the von Karman constant that has a magnitude of 0.4, u^* is the friction velocity of 0.67, z_0 is the aerodynamic roughness height of 0.4 m, and z is the height of wind speed measurement from the ground.

In the simulation, the turbulence intensity *I* was 1%, the

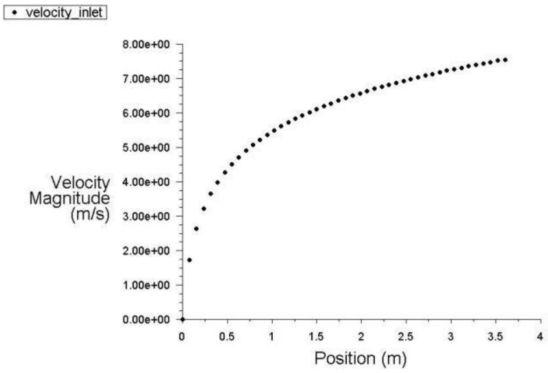

Fig. 13 Curve of the atmospheric boundary layer wind speed at the entrance boundary that changes with height

turbulence integral scale L_0 was 0.6 m, and the pressure variable was under a zero gradient boundary condition. The outlet boundary adopted the pressure outlet. Symmetric boundary conditions were applied to the upper surface and side surface of the computational domain. The bottom surface boundary condition of the computational domain was set as the non-slip wall that is simulated in exposure category *B* with a roughness height of 0.4 m and a roughness coefficient of 0.75.

3.3 Validation

The formula for the wind pressure coefficient uses the incoming wind velocity at the top of the model as the reference wind velocity. The formula for the wind pressure coefficient at the measuring point is as follows

$$C_p = \frac{P - P_\infty}{0.5\rho U^2} \qquad (2)$$

Where, C_p is the wind pressure coefficient at the measuring point, P is the wind pressure at the measuring point, P_∞ is the static pressure at the reference height, ρ is the inflow air density, and U is the average wind speed at the top of the building.

In the simulation, U=4.65 m/s. The grid independence test of the wind load parameters is shown in Table 2.

Case2 demonstrated that as the cell increased, the minimum negative wind pressure coefficient and aerodynamic lift coefficient did not change significantly. Therefore, the numerical simulation of the three-dimensional flow field would be unaffected by the numbers of cells, if the number of cells is above 1.75 million. The subsequent calculation used the Case2 grid marked with *.

In the grid independence test, the main flow field characteristics of Case2 were basically the same as that of Case1 and Case3. Meanwhile, the curve of the wind pressure coefficient along the centre line of the windward face, roof, and leeward face was almost the same, except that there was a slight difference in the wind pressure coefficient at the leading edge of the roof. Therefore, it was concluded that the Case2 grid was sufficient for independent flow field simulations.

The numerical simulation results of this paper were

Table 2 The grid independence test for the flat roof model

Case	Number of cells	Grid size of Zone1	Mesh size of Zone1	Minimum negative pressure coefficient	Lift coefficient
Case1	733,620	0.3 m	0.8 m	-0.83	0.0062
Case2*	1,759,620	0.2 m	0.8 m	-0.75	0.0068
Case3	3,757,620	0.15 m	0.8 m	-0.71	0.0072

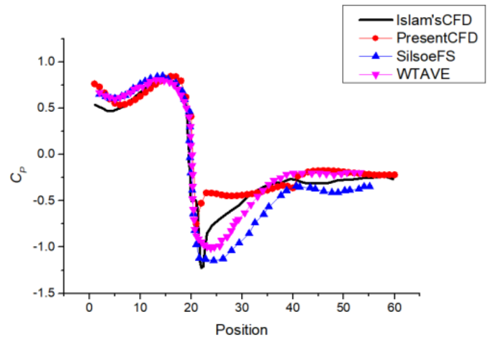

(a)

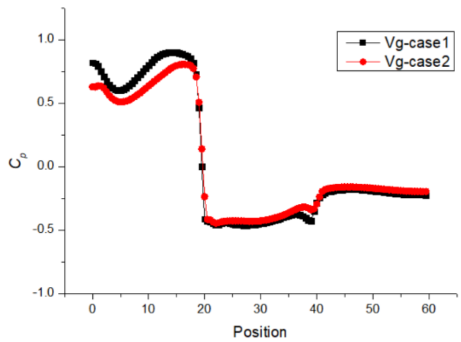

(b)

Fig. 14 Wind pressure coefficient along the centre line of the surface (a) without VG and (b) with VGst

compared with the numerical simulations of Abohela (Abohela, Hamza *et al.* 2013), the wind tunnel test results of SilsoeFS (Richards, Hoxey *et al.* 2001), and the average data results of 15 wind tunnel experiments by Hölscher and Niemann(WTAVE) (Hölscher and Niemann 1998). As shown in Fig. 14, the wind pressure coefficient with 60 measuring points along the centre line y=0 on the windward surface, roof, and leeward side were compared to others. As observed from the figure, the data from these numerical simulations were almost same as the simulation and wind tunnel experiments conducted by others. Therefore, it was concluded that the numerical simulation results of the flat roof were credible.

The grid independence test of the VG cases was also performed (see Fig. 14(b)). In Fig. 14(b), the Vg-case1 represents the coarse grid case with VGs (about 2.3 M cells); the Vg-case2 represents the refined grid case with VGs (about 3.0 M cells). It shows that pressure coefficient of Vg-case1 were almost the same as that of Vg-case2 along the centre line of the surface, except that there was a very slight difference at the windward surface. Therefore, it was concluded that the Vg-case1 grid was sufficient to give accurate flow field simulations.

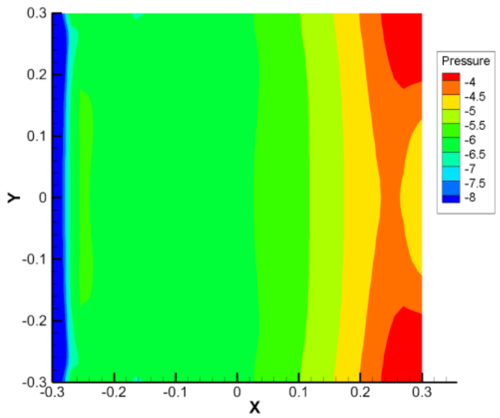

Fig. 15 Contour of pressure on the roof with no flow control

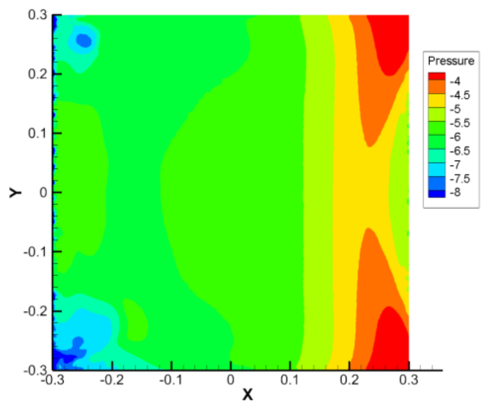

Fig. 16 Contour of pressure on the roof with flow control

4.2 Influence of VG parameters on wind pressure control

4.2.1 Influence of VG height on wind pressure control

B is the width of the roof (B=0.6 m), and the VGs were arranged in a single row on the top of the windward side. The size parameters were set as follows: l_a=0.02 m, l_b=0.06 m, l_c=0.06 m, θ=18°, λ=0.25 m. The changes in the wind pressure coefficient along the roof centre line y=0 at different VG heights are shown in Fig. 17, and the location of the measurement points is shown in Fig. 4. The contours of roof wind pressure with the different height of VGs are shown in Fig. 18.

As shown in Fig. 17, a strong negative wind pressure was generated at the leading area of the roof facade without the VGs. When the vortex generators were installed on the top of the windward facade with a vortex generator height h = 0.03 m (1/20 B), the negative wind pressure coefficient at the leading area of roof facade was greatly increased by approximately 40% which indicates that the vortex generators were effective at increasing the minimum negative wind pressure at the leading area of the roof.

Fig. 18 demonstrates that as the height of the VG increased from h = 0.01 m to h = 0.05 m, the negative wind pressure on both sides of the leading edge of the roof decreased. If the local negative wind pressure is relatively low and the strength of roof joint is not sufficient, the roof

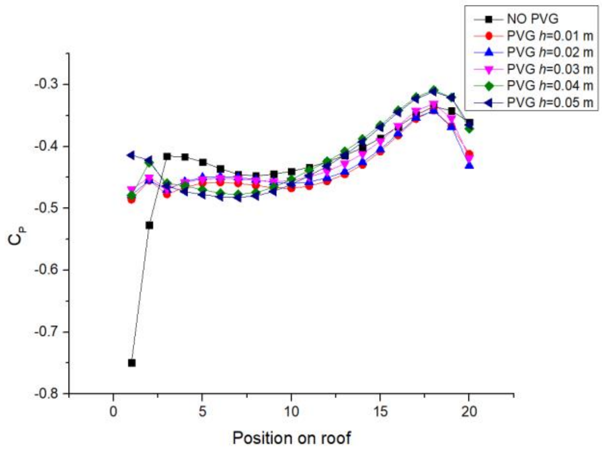

Fig. 17 Wind pressure coefficient changes along the roof centre line y = 0 under different VG heights

can be lifted up in the corner areas. This shows that h = 0.01 m (1/60 B) is the optimal size for VGs installed on a flat roof for wind resistance.

4.2.2 Influence of the VG row number on wind pressure control

The VG parameter sizes were set as follows:h=0.03 m, l_a=0.02 m, l_b=0.06 m, l_c=0.06 m, θ=18°, and λ=0.25 m. One row to three rows of VGs were arranged on the top of the windward facade and the vertical length between the vortex generators was d=0.1 m. Fig. 19 shows the wind pressure coefficient along the centre line y=0 on the roof with different vortex generators. Fig. 20 shows the contours of roof wind pressure with different rows of vortex generators

As illustrated in Fig. 19 and Fig. 20, the negative wind pressure coefficient at the leading area of roof facade increased by approximately 40% when the PVG was installed. However, when the number of rows of the vortex generator changed, the wind pressure coefficient had little effect. The negative wind pressure at the leading edge of the roof was changed by no more than 4.3%. The closer the vortex generator was to the separation point, the better the control effect on increasing the suction.

The reason for this phenomenon is that there is a stagnation point on windward facade while the bluff body flows around it. The stagnation point refers to the area where the velocity in the flow field is zero, and it is also the streamline dividing point of the flow (Corke 1979). With respect to the flow above the horizontal line of the stagnation point, it will flow upward to form a flow separation and a negative wind pressure region. For the flow below the horizontal line of the stagnation point, it will flow downward without forming a negative wind pressure region. In this simulation, the stagnation point was about 1/5 of the height from the top of the building and the pressure coefficient was 0.83. Therefore, only the vortex generator located above the stagnation point suppressed the separation and increased the negative wind pressure. The vortex generator located below the stagnation point could only disturb the flow field below the stagnation point and had no effect on the negative wind pressure on the roof.

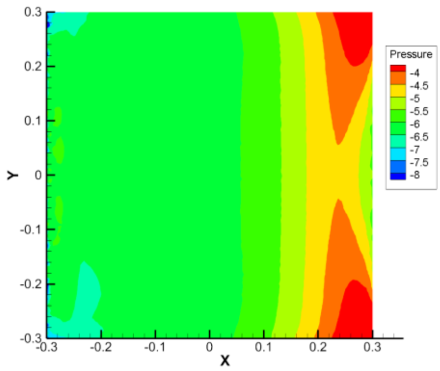

(a) h=0.01 m

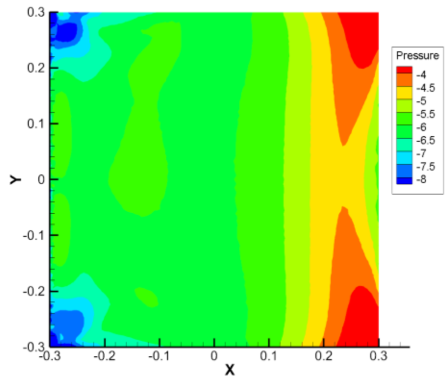

(b) h=0.02 m

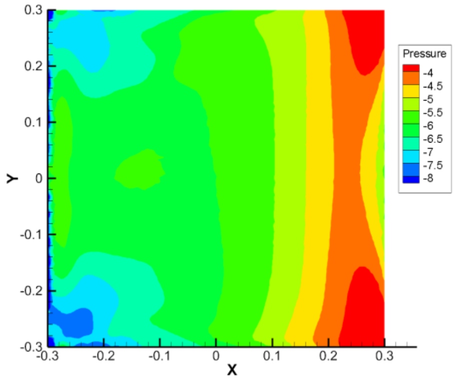

(c) h=0.03 m

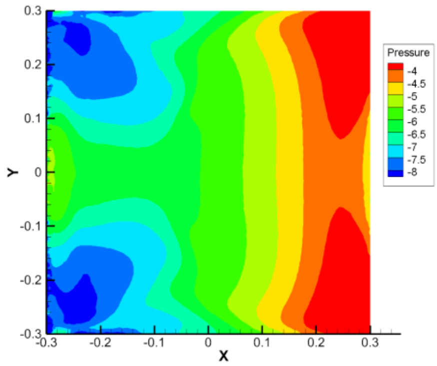

(d) h=0.04 m

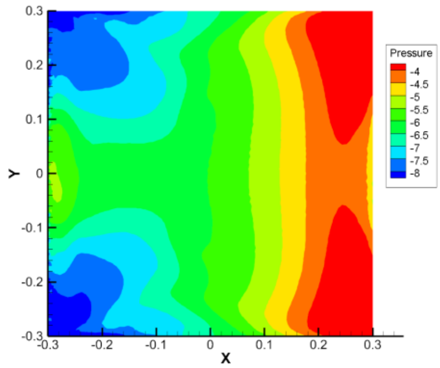

(e) h=0.05 m

Fig. 18 Contours of roof wind pressure at different VG heights

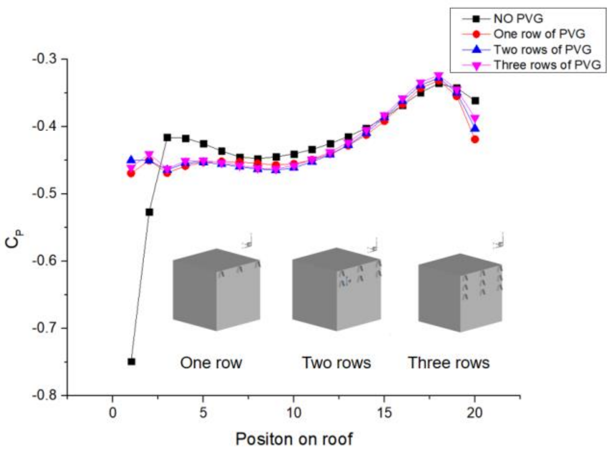

Fig. 19 Wind pressure coefficient changes with roof centre line y = 0 under different rows of VGs

4.2.3 Influence of vertical distance between the leading edge and trailing edge of VGs on wind pressure control

The VGs were arranged in a single row on the top of the windward facade. The parameter sizes were set as follows:h=0.03 m, l_a=0.02 m, l_b=0.06 m, θ=18°, and λ=0.25 m. As shown in Fig. 21, l_c (vertical distance between the leading edge and the trailing edge of the vortex generator) was adjusted. Fig. 22 shows the contours of roof wind pressure at different vertical distances between the leading edge and the trailing edge of the vortex generators.

As observed in Figs. 21 and 22, when the vertical distance between the leading edge and the trailing edge of the VGs were equal to 0.08 m, the negative wind pressure on both sides of the leading edge of the roof decreased sharply. An area of low negative wind pressure can lead to

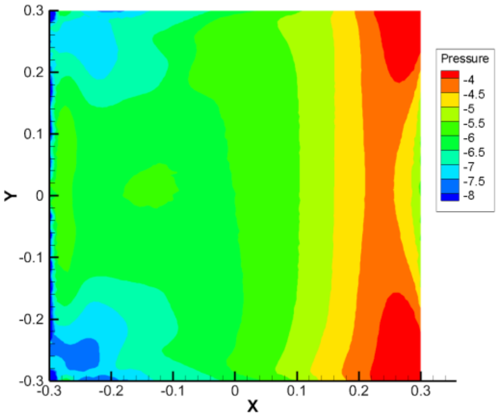

(a) One row of vortex generators

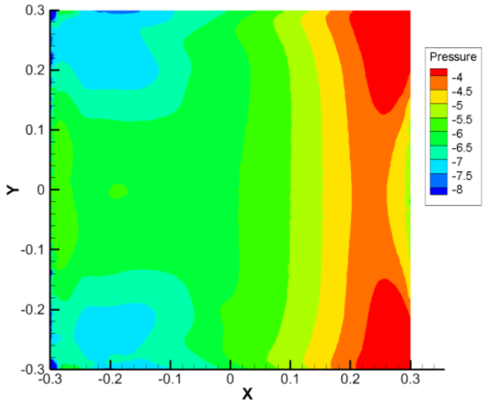

(b) Two rows of vortex generators

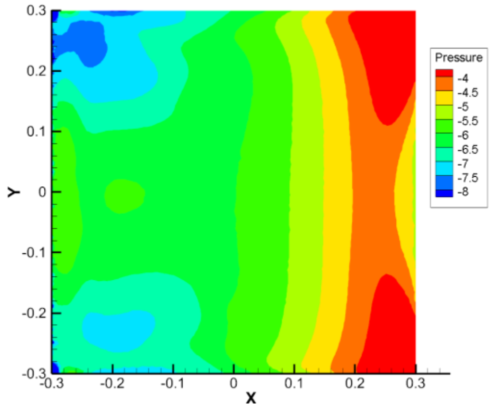

(c) Three rows of vortex generators

Fig. 20 Contour of roof wind pressure with different rows of VGs

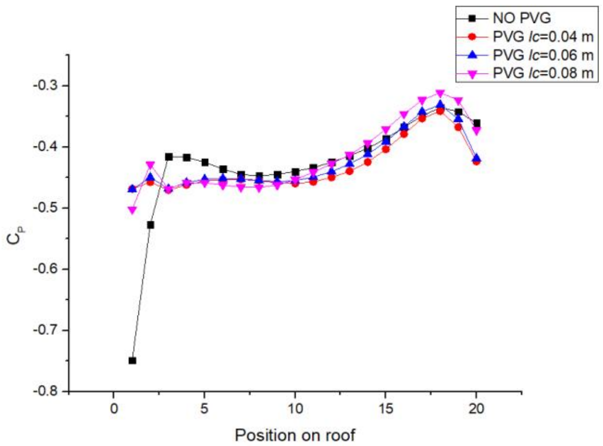

Fig. 21 Wind pressure coefficient changes with roof centre line y=0 under different vertical distances between the leading edge and the trailing edge of the VGs

to considerable wind suction on the roof and cause a flat roof to lift upwards. Therefore, l_c = 0.04 m (1/15 B) is the optimal size of VGs installed on a flat roof for wind resistance.

4.2.4 Influence of VG transverse spacing on wind pressure control

The VGs were arranged in a single row on the top of the windward facade. The parameter sizes were set as follows: h=0.03 m, l_a=0.02 m, l_b=0.06 m, l_c=0.06 m, and θ=18°.The lateral spacing (λ) of the vortex generator was adjusted. The wind pressure coefficient varied with the centre line y=0 of the roof and is illustrated in Fig. 23. The Fig. 24 shows contours of roof wind pressure at different transverse placement distances of VGs.

It can be seen in Figs. 23 and 24 that changing the lateral spacing of the vortex generator has little effect on the wind pressure coefficient when λ is less than 0.3 m (1/2 B). As the spacing of the roof is decreased from 5/12 B to 1/6 B, the wind pressure coefficient at the leading edge is changed only 4%. However, λ = 0.3 m (1/2 B) is not acceptable for C_p at leading edge of roof is about -0.65 which indicates less control effect by VGs. Therefore, for a flat roof cube model with a side length of 0.6 m, it is the best option to increase the negative wind pressure on the leading edge of roof when the lateral spacing of VGs is set to 5/12 B.

5. Conclusions

Placing VGs on the top of windward facade has been proposed in order to increase the negative wind pressure on the leading edge of a large span roof and improve the safety of the roof structure. This method can disturb the flow field, suppress the flow separation on the leading edge of the roof, and increase negative wind pressure on the leading edge of roof. A typical cube with a side length of 6 m was employed as the research object. In the present simulation, the scale ratio was 1/10, which was used to investigate the effectiveness of VGs, and the influences of vortex generator size parameters on negative wind pressure were discussed. The main conclusions are presented as follows:

- The vortex generators were highly effective at increasing the negative wind pressure on the leading edge of the flat roof. When the vortex generators were placed on the top of the windward facade and the size parameter of the vortex generator was h=0.03 m (h is the height of the vortex generator), l_a=0.02 m (l_a is the leading edge distance of the vortex generator), l_b=0.06 m (l_b is the trailing edge distance of the vortex generator), l_c=0.06 m (l_c is the vertical distance between the leading edge and the trailing edge of the vortex generator θ=18° (θ is the angle between the vortex generator and the incoming flow) λ=0.25 m (λ is the horizontal distance between the vortex generators), the negative wind pressure coefficient on the leading edge of the roof greatly increased by approximately 40%.
- h=0.01 m (1/60 B, B is the width of the roof), l_c=0.04 m (1/15 B) and λ=0.25 m (5/12 B) were the optimal sizes for the vortex generators that exhibited effective control on increasing the negative wind pressure on the leading edge of the roof.
- The wind pressure control effect of the vortex generators was essentially unaffected by the arrangement of the row numbers of the vortex generators. In addition, the vortex generators were only effective at increasing the negative wind pressure on the leading edge of the roof when they were installed above the stagnation point.

Acknowledgments

This research was supported by the National Natural Science Foundation of China (No. 51878131), the Fundamental Research Funds for the Central Universities (No. 2572019BJ06)

References

Abohela, I., Hamza, N. and Dudek, S. (2013), "Effect of roof shape, wind direction, building height and urban configuration on the energy yield and positioning of roof mounted wind turbines", *Renew. Energy*. **50,** 1106-1118. https://doi.org/10.1016/j.renene.2012.08.068.

Baetke, F., Werner, H. and Wengle, H. (1990), "Numerical simulation of turbulent flow over surface-mounted obstacles with sharp edges and corners", *J. Wind Eng. Ind. Aerod*., **35**(1-3), 129-147. https://doi.org/10.1016/0167-6105(90)90213-V.

Beyers, J.H.M., Sundsbø, P.A. and Harms, T.M. (2004), "Numerical simulation of three-dimensional, transient snow drifting around a cube", *J. Wind Eng. Ind. Aerod.,* **92**(9) 725-747. https://doi.org/10.1016/j.jweia.2004.03.011.

Blocken, B., Stathopoulos, T. and Carmeliet, J. (2007), "CFD simulation of the atmospheric boundary layer: wall function problems", *Atmosp. Environ.*, **41**(2), 238-252. https://doi.org/10.1016/j.atmosenv.2006.08.019.

Browne, M.T.L., Gibbons, M.P.M., Gamble, S. and Galsworthy, J. (2013), "Wind loading on tilted roof-top solar arrays: The parapet effect", *J. Wind Eng. Ind. Aerod*., **123** 202-213. https://doi.org/10.1016/j.jweia.2013.08.013.

Corke, T.C., Nagib, H.M. (1979), "Wind loads on a building model in a family of surface layers", *J. Wind Eng. Ind. Aerod*., **5**, 159-177. https://doi.org/10.1016/0167-6105(79)90029-1.

Cheng, Z., Lou, W., Sun, B. and Tang, J. (2000), "Wind load on roof structures and mechanism of wind-induced damages", *J. Build. Struct*., **21**(04), 39-47.

Gao, F., Wang, X. and Zhang, H. (2016), "A research on boundary layer control of asymmetric supersonic flow past micro-vortex generator", *J. Air Force Eng. Univ. Nat. Sci. Edit*., **17**(6), 6-11.

Gullbrekken, L., Uvsløkk, S., Kvande, T., Pettersson, K. and Time, B. (2018), "Wind pressure coefficients for roof ventilation purposes", *J. Wind Eng. Ind. Aerod*., **175** 144-152. https://doi.org/10.1016/j.jweia.2018.01.026.

Hölscher, N. and Niemann, H.J. (1998), "Towards quality assurance for wind tunnel tests: A comparative testing program of the Windtechnologische Gesellschaft", *J. Wind Eng. Ind. Aerod*., **74-76,** 599-608. https://doi.org/10.1016/S0167-6105(98)00054-3.

Lee, M., Lee, S.H., Hur, N. and Choi, C.K. (2010), "A numerical simulation of flow field in a wind farm on complex terrain", *Wind Struct.,* **13**(4), 375-383.

Lin, J.C. (2002), "Review of research on low-profile vortex generators to control boundary-layer separation", *Progress in Aerospace Sciences*. **38**(4), 389-420. https://doi.org/10.1016/S0376-0421(02)00010-6.

Manolesos, M. and Voutsinas, S.G. (2015), "Experimental investigation of the flow past passive vortex generators on an airfoil experiencing three-dimensional separation", *J. Wind Eng. Ind. Aerod*., **142** 130-148. https://doi.org/10.1016/j.jweia.2015.03.020.

Moravej, M., Irwin, P., Zisis, I., Chowdhury, A.G. and Hajra, B. (2017), "Effects of roof height on local pressure and velocity coefficients on building roofs", *Eng. Struct*., **150** 693-710. https://doi.org/10.1016/j.engstruct.2017.07.083.

Richards, P.J., Hoxey, R.P. and Short, L.J. (2001), "Wind pressures on a 6 m cube", *J. Wind Eng. Ind. Aerod*., **89**(14), 1553-1564.

Oliveira N.L.D. and Fernando M.D.S. (2018), "Simulation and measurements of wind interference on a solar chimney performance", *J. Wind Eng. Ind. Aerod*., **179**, 135-145. https://doi.org/10.1016/j.jweia.2018.05.020.

Rizzo, F. and Ricciardelli, F. (2017), "Design pressure coefficients for circular and elliptical plan structures with hyperbolic paraboloid roof", *Eng. Struct*., **139** 153-169. https://doi.org/10.1016/j.engstruct.2017.02.035.

Shan, W., Tamura, Y., Yang, Q. and Li, B. (2018), "Effects of curved slopes, high ridges and double eaves on wind pressures on traditional Chinese hip roofs", *J. Wind Eng. Ind. Aerod.*, **183** 68-87. https://doi.org/10.1016/j.jweia.2018.10.010.

Stillfried, F.V., Wallin, S. and Johansson, A. (2010). "An improved passive vortex generator model for flow separation control", *Flow Control Conference*. https://doi.org/10.2514/6.2010-5091.

Xin, D., Zhang, H. and Ou, J. (2018), "Experimental study on mitigating vortex-induced vibration of a bridge by using passive vortex generators", *J. Wind Eng. Ind. Aerod*., **175** 100-110. https://doi.org/10.1016/j.jweia.2018.01.046.

TK